Hydrothermal synthesis of TiO_2/reduced graphene oxide nanocomposite with enhanced photocatalytic activity

Guoe Cheng, Yu Zhang, Hanzhong Ke, Tingting Hao, Youzhi Wang

Faculty of Material Science & Chemistry, China University of Geosciences, Wuhan, Hubei 430074, People's Republic of China
E-mail: kehanz@163.com

Published in Micro & Nano Letters; Received on 14th May 2014; Revised on 8th October 2014; Accepted on 17th October 2014

The composite of peanut-like TiO_2 nanoparticles and reduced graphene oxide (rGO) was successfully synthesised via a facile one-step hydrothermal method in mixed solvents of diethanol amine and distilled water. The crystallite, morphology and structure features of the composite were characterised by X-ray diffraction, Brunauer-Emmett-Teller specific area analysis, transmission electron microscopy and high-resolution transmission electron microscopy. The results indicated that the as-synthesised TiO_2 was of peanut-like shape with about 21–32 nm in length and was anchored on the surface of the rGO sheet. In addition, the TiO_2/rGO composite presented excellent photocatalytic activity of rhodamine B under visible light irradiation compared with commercial Degussa P25. A proposed mechanism for the photocatalytic process is also discussed.

1. Introduction: TiO_2 is one of the most promising metal semiconductor materials that exhibits photocatalytic activity and is widely used in environmental protection [1, 2]. When illuminated by light, TiO_2 generates electron–hole pairs that can create O^{2-} and OH radicals to decompose pollutants. However, the fast recombination of photogenerated electrons and holes restricts its photocatalytic application. A number of strategies have been proposed to overcome this limitation. Doping with noble metals (e. g. Pt, Au, Pd) [3, 4] can restrain the recombination of electron–hole pairs. However, the high cost has become an obstacle in its application. In addition, semiconductor composite materials such as CdS/TiO_2 nanocomposite can also decrease the recombination of electron–hole pairs. However, the release of cadmium in solution may cause additional environmental pollution [5].

In recent years, nanocarbon materials such as carbon nanotubes and C_{60} have attracted attention in photocatalytic fields since carbon can efficiently separate the electron–hole pairs. Unfortunately, the high production cost and the weakening of light intensity arriving at the surface of catalysts limit the potential application on a large scale [6]. In comparison, graphene provides a high surface area and high electron mobility, thereby accelerating the transfer of photogenerated electrons to the pollutant [6, 7]. Owing to the low economical cost and easy preparation, graphene has attracted significant attention for various applications [6, 8]. In the reported TiO_2/graphene composite literature, TiO_2/graphene composites show significant enhancement photocatalytic efficiency because of the electron transfer from TiO_2 to graphene, which promotes charge separation and stabilisation [9–12]. Zhang *et al.* [10] prepared a TiO_2 nanoparticle–graphene composite and report enhanced photocatalytic activity for the degradation of methylene blue. Pan *et al.* [11] found that the photocatalytic activity of graphene–TiO_2 nanowire nanocomposite is much higher than graphene–TiO_2 nanoparticle composite and pure TiO_2 nanowires or TiO_2 nanoparticles. Perera *et al.* [12] reported a facile route for the growth of TiO_2 nanotubes on reduced graphene oxide (rGO) sheets and found that the composites with 10% rGO show the highest photocatalytic activity, with a three-fold enhancement in photocatalytic efficiency over pure TiO_2 nanotubes. These reports illustrate that the photocatalytic performance of graphene–TiO_2 composites are significantly related to the graphene content, the degree of interfacial contact, the heterojunction between graphene and TiO_2 and the surface area of TiO_2 nanocrystals. The research on the synthesis of TiO_2/rGO nanocomposites is still worthy of exploring in greater depth. Herein, we report a facile route and robust one-step synthesis of peanut-like TiO_2/rGO composite with enhanced photocatalytic activity of rhodamine B (RhB) under visible light irradiation.

2. Experimental

2.1. Preparation of TiO_2/rGO: Graphene oxide (GO) was prepared from graphite powder using a modified Hummer's method [13]. The TiO_2/rGO composite was synthesised by a facile hydrothermal method. In a typical procedure, 6 mg of as-prepared GO was dispersed in 40 ml distilled water and sonicated for 30 min. Thereafter, 0.500 g of $(NH_4)_2TiF_6$ powder was added into the above GO solution and 20 ml of diethanol amine was gradually added under stirring. Finally, the obtained brown solution was transferred into a Teflon-coated stainless steel autoclave and heated at 180°C for 12 h. After cooling to room temperature, the brown precipitates were collected and washed with distilled water and absolute ethanol several times by ultrasonication and centrifugation, and dried at 60°C for 24 h. For comparison, bare TiO_2 was synthesised by a similar procedure except for the absence of GO.

2.2. Characterisation: The microscopic nanostructures were observed by transmission electron microscopy (TEM; FEI Tecnai G^2 20 operated at 200 kV) and high-resolution transmission electron microscopy (HRTEM; JEM-2010FEF operated at 200 kV). The crystallite structures of the materials were investigated by X-ray powder diffraction analysis (XRD, Bruker Axs D8-Focus, Cu Kα radiation with $\lambda = 1.5406$ Å). The specific surface area and pore-size distribution were characterised by analysing the N_2 adsorption and desorption isotherms using Micrometrics ASAP 2000 equipment.

2.3. Photocatalytic activity measurement: The photocatalytic performances of the catalysts were evaluated by the degradation of RhB under visible light irradiation using a 500 W Xe lamp with a 420 nm cutoff filter. Typically, 20 mg of catalysts was dispersed in 50 ml of 10 mg/l RhB aqueous solution in a quartz tube. Prior to irradiation, the suspension was magnetically stirred for 60 min in the dark to favour the adsorption–desorption equilibration. Every time, 5 ml of the above solution was taken out and centrifuged before UV–vis analysis. UV–vis adsorption

doi: 10.1049/mnl.2014.0238

spectra were recorded by the UV–vis spectrum (UV-1801) of RhB at the maximum absorbance of 554 nm at certain time intervals (20 min) to monitor the process.

3. Result and discussion: Fig. 1 illustrates the X-ray diffraction (XRD) patterns of GO, bare TiO_2 and TiO_2/rGO composite, respectively. The diffraction pattern of GO shows a characteristic (002) peak at $2\theta = 10.5°$ without other peaks, which indicates that the pristine graphite is oxidised into GO with a well-ordered, lamellar structure (Fig. 1*a*). As shown in Fig. 1*b*, the presence of characteristic peaks at about 25.3°, 37.9°, 47.8° and 54.4° are observed, which are identical to the standard cards (JCPDS Card No. 21-1272) of the anatase phase of TiO_2. Meanwhile, the weak peak at $2\theta = 30.7°$ in the sample suggests the presence of a small quantity of brookite TiO_2, which is frequently observed as a byproduct of the anatase [5]. Fig. 1*c* shows a diffraction pattern similar to that of bare TiO_2. It should be noted that there are no observable peaks of GO in the composite. During the hydrothermal process, GO is usually reduced to rGO [14]. Furthermore, the low content of rGO in the composite could also be an important factor [15].

The morphologies and microstructures of the obtained samples were investigated by TEM. As shown in Fig. 2*a*, the GO sheets are not flat but crumpled with a layered structure. The morphology of TiO_2 nanocrystals is characterised as peanut-like shapes with about 21–32 nm in length (Fig. 2*b*). After hydrothermal reaction together with GO, its morphology is scarcely changed. The peanut-like TiO_2 nanoparticles are found to be uniformly anchored on the surface of the rGO sheet (in Fig. 2*c*), indicating the formation of TiO_2/rGO nanocomposite. In addition, the edge of rGO can be easily observed. The corresponding HRTEM image (in Fig. 2*d*) shows clear lattice fringes, which also suggests that the TiO_2 nanoparticle is a single crystal. The lattice spacing of the TiO_2 is about 0.352 nm, corresponding to the anatase (101) planes.

To evaluate the pore structure and the pore size of the composite, the N_2 adsorption–desorption isotherms were investigated. As shown in Fig. 3, both the isotherms of the samples are of classical type IV with an H1 hysteresis loop, which imply the presence of mesoporous structures in the materials. It is noteworthy that both bare TiO_2 and TiO_2/rGO composite have a large specific surface area (144.4 m^2g^{-1} for bare TiO_2 and 138.3 m^2g^{-1} for the TiO_2/rGO composite). There are no significant changes in the Brunauer-Emmett-Teller-Specific areas of the photocatalysts, possibly because of the low content of rGO in the TiO_2/rGO composite. The TiO_2/rGO composite does not merely result in simple physical adsorption but also largely relates to the selective adsorption of aromatic rings on the TiO_2 nanoparticles. The adsorption is non-covalent and driven by $\pi - \pi$ stacking between TiO_2 nanoparticles and the aromatic regions of the rGO [16]. We calculated the

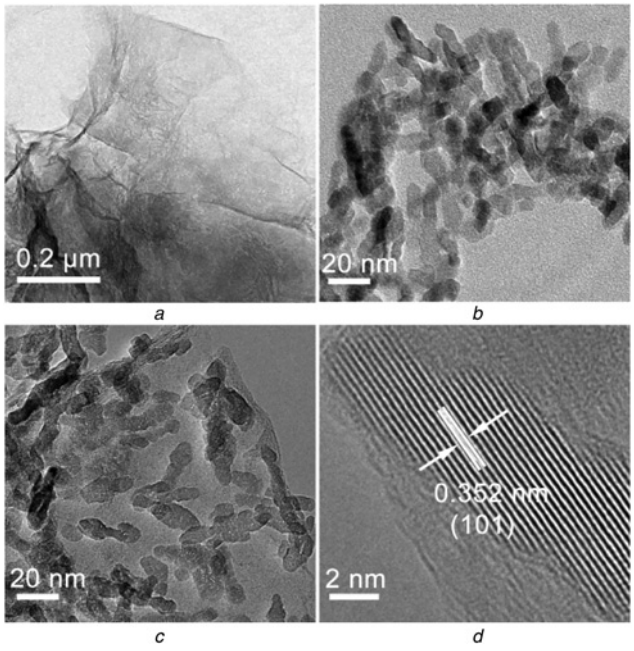

Figure 2 *TEM images of GO, bare TiO_2 and TiO_2/rGO composite, and HRTEM image of TiO_2/rGO composite*
a TEM image of GO
b TEM image of Bare TiO_2
c TEM image of TiO_2/rGO composite
d HRTEM image of TiO_2/rGO composite

pore-size distribution by the Barrett-Joyner-Halenda method from the desorption branch of the isotherm. The pore-size distribution of bare TiO_2 shows a narrow range of 5.0–16.0 nm with a maximum pore diameter of 10.2 nm. These mesopores are from the aggregation of primary particles. The narrow pore distributions also imply that the prepared bare TiO_2 particles have a uniform particle size distribution. Compared with the bare TiO_2, the TiO_2/rGO composite shows a similar pore-size distribution in the range of 5.0–16.0 nm, while another sharp peak located at 3.88 nm related to rGO can be observed. The presence of small-size mesopores can positively reflect in the photocatalytic activity.

Fig. 4 displays the photodegradation efficiencies of RhB with different catalysts under visible light irradiation. It could be observed that bare TiO_2 shows a little higher catalytic efficiency than P25. However, in the presence of a TiO_2/rGO composite, photodegradation is remarkably enhanced. The photodegradation of RhB with TiO_2/rGO is about 73% within 120 min under visible light irradiation while that of P25 is 46%. This excellent photocatalytic

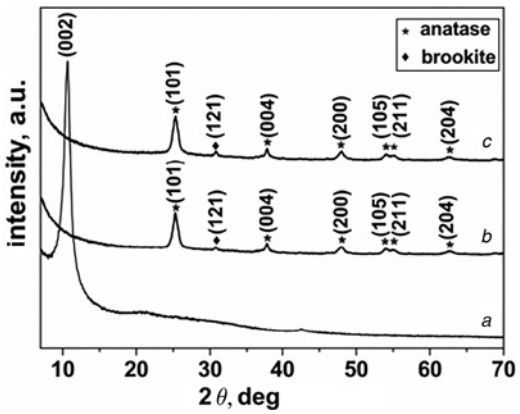

Figure 1 *XRD patterns of GO, bare TiO_2, and TiO_2/rGO composite*
a GO; *b* Bare TiO_2; *c* TiO_2/rGO

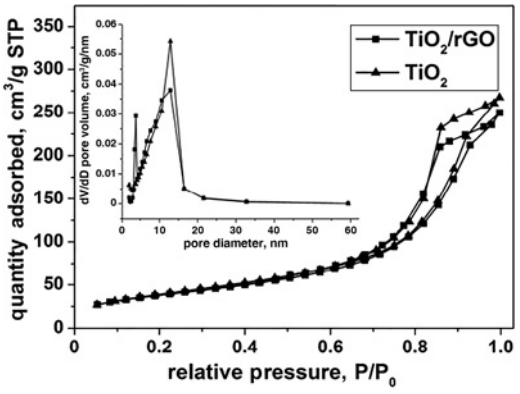

Figure 3 *Nitrogen adsorption and desorption isotherms for bare TiO_2 and TiO_2/rGO composite*
Inset: Corresponding pore-size distribution

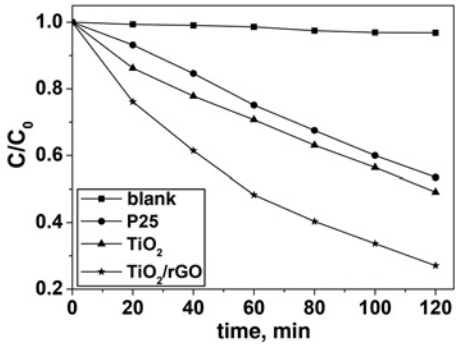

Figure 4 *Comparison of photocatalytic activity of the samples for degradation of RhB solution*

activity cannot merely relate to the crystal phase, unique structure and special surface area, but also largely attributed to the transport of charge carriers. Under visible light irradiation, TiO_2 particles absorb photons to generate electron–hole (e^-/h^+) pairs. Electrons are photoexcited to the conduction band, leaving positively charged holes in the valence band. Considering the calculated work function of graphene is 4.42 eV and the CB position of anatase is about −4.21 eV with a bandgap of about 3.2 eV, the photogenerated electron transfer from TiO_2 to graphene is favourable [17]. It has been documented that the reduction of GO by the hydrothermal method causes oxygen sites to remain which can accept electrons and undergo reduction during the process of photocatalysis, indicating that rGO effectively suppresses the probability of electron–hole recombination. In addition, rGO possesses an excellent ability of electronic transmission because of its giant π-conjugation system and two-dimensional planar-conjugation structure. Hence, the rapid transmission of electrons could effectively accelerate the photogenerated e^-/h^+ pairs separation. Overall, the electron-accepting and electron-transporting properties of rGO in the composite hinders the recombination of charge carriers, which enhances the photocatalytic activity [15].

4. Conclusion: In summary, we have developed a facile hydrothermal route for the synthesis of peanut-like TiO_2/rGO composite in the mixed solvents of diethanol amine and distilled water. The TiO_2/rGO composite exhibits significantly higher photocatalytic activity than P25. The enhanced photocatalytic activity is attributed to the excellent electron accepting and transporting properties of rGO, which is favourable for the separation of photogenerated electrons and holes. It is expected that the TiO_2/rGO composite can act as a superior photocatalyst for practical applications in environmental pollutant management.

5 References

[1] Lu C.H., Wu W.H., Kale R.B.: 'Microemulsion-mediated hydrothermal synthesis of photocatalytic TiO_2 powders', *J. Hazard. Mater.*, 2008, **154**, pp. 649–654

[2] Chen R., Wang M.: 'Synthesis of hierarchical TiO_2 micro/nanostructure and its application in hybrid solar cell', *Mater. Lett.*, 2012, **69**, pp. 41–44

[3] Linic S., Christopher P., Ingram D.B.: 'Plasmonic-metal nanostructures for efficient conversion of solar to chemical energy', *Nat. Mater.*, 2011, **10**, pp. 911–921

[4] Liu L., Ji Z., Zou W., *ET AL.*: 'In situ loading transition metal oxide clusters on TiO_2 nanosheets as co-catalysts for exceptional high photoactivity', *ACS Catal.*, 2013, **3**, pp. 2052–2061

[5] Štengl V., Popelková D., Vláčil P.: 'TiO_2–graphene nanocomposite as high performace photocatalysts', *J. Phys. Chem. C*, 2011, **115**, pp. 25209–25218

[6] Bai S., Shen X.: 'Graphene–inorganic nanocomposites', *RSC Adv.*, 2012, **2**, pp. 64–98

[7] Chen X., Shen S., Guo L., Mao S.S.: 'Semiconductor-based photocatalytic hydrogen generation', *Chem. Rev.*, 2010, **110**, pp. 6503–6570

[8] Shen J., Yan B., Shi M., Ma H., Li N., Ye M.: 'One step hydrothermal synthesis TiO_2-reduced graphene oxide sheets', *J. Mater. Chem.*, 2011, **21**, p. 3415

[9] Wang F., Zhang K.: 'Reduced graphene oxide–TiO_2 nanocomposite with high photocatalystic activity for the degradation of rhodamine B', *J. Mol. Catal. A, Chem.*, 2011, **345**, pp. 101–107

[10] Zhang H., Lv X.J., Li Y.M., Wang Y., Li J.H.: 'P25-graphene composite as a high performance photocatalyst', *ACS Nano*, 2010, **4**, pp. 380–386

[11] Pan X., Zhao Y., Liu S., Korzeniewski C.L., Wang S., Fan Z.: 'Comparing graphene-TiO_2 nanowire and graphene-TiO_2 nanoparticle composite photocatalysts', *ACS Appl. Mater. Interfaces*, 2012, **4**, pp. 3944–3950

[12] Perera S.D., Mariano R.G., Vu K., *ET AL.*: 'Hydrothermal synthesis of graphene-TiO_2 nanotube composites with enhanced photocatalytic activity', *ACS Catal.*, 2012, **2**, pp. 949–956

[13] Zhang Y., Pan C.: 'TiO_2/graphene composite from thermal reaction of graphene oxide and its photocatalytic activity in visible light', *J. Mater. Sci.*, 2011, **46**, pp. 2622–2626

[14] Chai B., Li J., Xu Q., Dai K.: 'Facile synthesis of reduced graphene oxide/WO_3 nanoplates composites with enhanced photocatalytic activity', *Mater. Lett.*, 2014, **120**, pp. 177–181

[15] Sher Shah M.S.A., Park A.R., Zhang K., Park J.H., Yoo P.J.: 'Green synthesis of biphasic TiO_2–reduced graphene oxide nanocomposites with highly enhanced photocatalytic activity', *ACS. Appl. Mater. Interfaces*, 2012, **4**, pp. 3893–3901

[16] Yoo D.H., Cuong T.V., Pham V.H., *ET AL.*: 'Enhanced photocatalytic activity of graphene oxide decorated on TiO_2 films under UV and visible irradiation', *Curr. Appl. Phys.*, 2011, **11**, pp. 805–808

[17] Zhou K., Zhu Y., Yang X., Jiang X., Li C.: 'Preparation of graphene–TiO_2 composites with enhanced photocatalytic activity', *New J. Chem.*, 2011, **35**, pp. 353–359

doi: 10.1049/mnl.2014.0238